


## Directly tunable magnon frequency comb effect based on domain wall

Xiaoxue Yang(杨霄雪), Huiting Li(李慧婷), Xue-Feng Zhang(张雪枫), Xiao-Ping Ma(马晓萍), Je-Ho Shim(沈帝虎), Yingjiu Jin(金迎九), and Hong-Guang Piao(朴红光)

**Citation:**Chin. Phys. B, 2025, 34 (**10**): 107507. DOI: 10.1088/1674-1056/ade856
http://cpb.iphy.ac.cn; http://iopscience.iop.org/cpb

**What follows is a list of articles you may be interested in**

---

## A design for an antiferromagnetic material based on self-assembly for information storage

Si-Yan Gao(高思妍), Yi-Feng Zheng(郑益峰), Shu-Qiang He(何述强), Haiping Fang(方海平), and Yue-Yu Zhang(张越宇)

Chin. Phys. B, 2025, 34 (**6**): 067504. DOI: 10.1088/1674-1056/adc6f5

## Direct observation of ultrafast magnetization dynamics in Co/Ni bit patterned media by time-resolved scanning Kerr microscopy

Wei Zhang(张伟), Wei He(何为), Qin-Li Lv(吕琴丽), Jian-Wang Cai(蔡建旺), Xiang-Qun Zhang(张向群), and Zhao-Hua Cheng(成昭华)

Chin. Phys. B, 2025, 34 (**4**): 047501. DOI: 10.1088/1674-1056/adb67e

## Dzyaloshinskii-Moriya interaction and field-free sub-10 nm topological magnetism in Fe/bismuth oxychalcogenides heterostructures

Yaoyuan Wang(王垚元), Long You(游龙), Kai Chang(常凯), and Hongxin Yang(杨洪新)

Chin. Phys. B, 2024, 33 (**9**): 097508. DOI: 10.1088/1674-1056/ad6a0e

## Mapping the antiparallel aligned domain rotation by microwave excitation

Jing Zhang(张景), Yuanzhi Cui(崔远志), Xiaoyu Wang(王晓雨), Chuang Wang(王创), Mengchen Liu(刘梦晨), Jie Xu(徐洁), Kai Li(李凯), Yunhe Zhao(赵芸鹤), Zhenyan Lu(陆振烟), Lining Pan(潘丽宁), Chendong Jin(金晨东), Qingfang Liu(刘青芳), Jianbo Wang(王建波), and Derang Cao(曹德让)

Chin. Phys. B, 2024, 33 (**9**): 097506. DOI: 10.1088/1674-1056/ad5536

## RKKY interaction in helical higher-order topological insulators

Sha Jin(金莎), Jian Li(李健), Qing-Xu Li(李清旭), and Jia-Ji Zhu(朱家骥)

Chin. Phys. B, 2024, 33 (**7**): 077503. DOI: 10.1088/1674-1056/ad3ef9

---

**SPECIAL TOPIC — Advanced magnonics**

# Directly tunable magnon frequency comb effect based on domain wall

Xiaoxue Yang(杨霄雪)[1,2], Huiting Li(李慧婷)[1,2], Xue-Feng Zhang(张雪枫)[1,2], Xiao-Ping Ma(马晓萍)[1,2,†], Je-Ho Shim(沈帝虎)[1,2], Yingjiu Jin(金迎九)[1,2], and Hong-Guang Piao(朴红光)[1,2,‡]

[1] *Department of Physics, College of Science, Yanbian University, Yanji* 133002, *China*
[2] *Institute of Quantum Science and Technology, Yanbian University, Yanji* 133002, *China*

(Received 8 April 2025; revised manuscript received 14 June 2025; accepted manuscript online 26 June 2025)

Magnon frequency combs have garnered significant attention due to their wide-ranging potential applications, primarily generated by the interplay between spin waves and oscillating magnetic textures. Developing an easily achievable magnon frequency comb with directly tunable comb spacing is pivotal for broadening its utility. In this study, we engineered a Bloch-type magnetic domain wall with a stable structure and fixed position by employing a dual-pinning approach utilizing artificial structural defects and stray fields. We established a magnetic domain wall oscillation mode based on resonant Larmor precession, serving as the foundation for a magnon frequency comb derived from magnetic domain walls. By leveraging the locally distributed Oersted field generated by an alternating current, we achieved precise control over the oscillation frequency of the domain wall, thereby realizing a magnon frequency comb with directly tunable comb spacing. The insights from this research offer a promising shortcut for exploring frequency combs based on the interaction between spin waves and magnetic domain walls.

**Keywords:** spintronics, magnetic domain wall, spin waves, frequency comb

**PACS:** 75.40.Gb, 75.60.Ch, 85.75.–d, 91.30.Bi

**DOI:** 10.1088/1674-1056/ade856 **CSTR:** 32038.14.CPB.ade856

## 1. Introduction

Frequency comb refers to a series of discrete and equidistant comb-like spectral lines in the frequency spectrum of a signal. Recently, these unique spectral structures have been discovered successively in electromagnetic wave and spin-wave (SW) systems. Among them, magnon frequency combs (MFCs) have garnered significant attention due to their broad application prospects in microwave precision measurement,[1,2] logical defect detection,[3] magnetic sensors,[4,5] as well as magnon lasers and magnon quantum computing.[6,7] The MFC effect is typically realized through the nonlinear interaction between SWs and magnetic textures,[6,8] where the fundamental frequency of the spectrum corresponds to that of the SWs. At the same time, the equidistant comb-like spectral lines represent sum and difference frequencies generated by multiple couplings between the SWs and oscillating magnetic textures. Existing researches predominantly focus on MFCs based on interactions between SWs and zero-dimensional magnetic textures such as skyrmions[9–11] and magnetic vortices.[7,12] In contrast, studies on frequency combs induced by magnetic domain walls (DWs)[1,13,14] remain relatively scarce. One reason is that DW oscillation often involves coupled nonlinear oscillations in size, position, and internal magnetization states,[15–21] which collectively impair frequency comb performance. For instance, although Walker breakdown precession can easily cause vibration of magnetic DWs,[5,22–24] when the external driving field exceeds a certain threshold, the vibration DWs will move, leading to creep motion,[18,25] or the DW configuration will undergo a magnetized precession transition between Bloch and Néel configurations or vortex.[17,20,23,26,27] In addition, positional shifts in DWs will induce a Doppler effect,[16] degrading the frequency comb's quality. Despite these drawbacks, it is noteworthy that, compared to magnetic skyrmions or vortices, DWs are more ubiquitous, easier to generate in magnetic systems, and have broader application requirements, making the study of MFCs based on DWs particularly important. As mentioned earlier, the oscillation of magnetic DW is complex, so a critical aspect of MFC research based on DWs is how to simplify the DW oscillation to minimize noise. Existing researches generally employ the introduction of pinning sites to restrain the movement of the DW.[4,5,24,27–30] In this study, we introduce a dual-pinning mechanism combining geometric confinement and localized stray fields to simultaneously control the positional stability and magnetization uniformity of DWs, thereby achieving high-performance MFC via the SW–DW interaction.

Another critical aspect of MFC research involves tuning the comb spacing by controlling the vibration frequencies of magnetic textures. Current research typically relies on altering the intrinsic vibration modes of magnetic textures, where

†Corresponding author. E-mail: xpma1222@ybu.edu.cn
‡Corresponding author. E-mail: hgpiao@ybu.edu.cn

© 2025 Chinese Physical Society and IOP Publishing Ltd. All rights, including for text and data mining, AI training, and similar technologies, are reserved.

the vibration frequencies are not only influenced by SW excitation frequencies,[11,31] but also primarily determined by the structure and material parameters of the magnetic system[10,32] and the characteristics of the applied physical fields.[9,10,29,33] Reported approaches for changing the comb spacing include applying AC current,[31,34] spin–orbit torque[13] or alternating magnetic fields.[2,9,14] However, these methods indirectly modulate the vibration frequencies of magnetic textures, and their regulatory effects are significantly affected by other related factors. We hypothesize that if a magnetic DW undergoes forced vibrations under an external magnetic field, its vibration frequency could be directly dictated by the frequency of the driving field, thus enabling precise control of comb spacing. Although the global magnetic field is the most straightforward driver and readily available means to induce DW vibrations, it can also alter the propagation characteristics of SWs, thereby introducing instability. If a nanoscale localized magnetic field can be generated to act exclusively on the region where the DW is located, the above mentioned issue could be mitigated effectively.

Based on this hypothesis, this study utilizes the localized Oersted field generated by microscale distributed current to control DW oscillations directly and proposes an MFC mechanism with tunable comb spacing. For the first step, using micromagnetic simulations, we investigate frequency comb generation from SW–DW interactions without applying any external field. We further explore the influence of the localized Oersted field distributed within the magnetic DW region on the MFC. By adjusting the frequency/amplitude of the current to change the Oersted field acting on the magnetic DW region, precise regulation of the comb spacing is achieved. The methods and conclusions presented in this study provide a beneficial approach for advancing frequency comb research based on SW–DW interactions.

## 2. Micromagnetic simulation

We perform the micromagnetic simulations using Mumax3,[35] considering a CoFeB ferromagnetic thin film with perpendicular magnetic anisotropy (PMA). The dimension of the film is set to $1000 \times 20 \times 1$ nm$^3$, with a cell size of $1 \times 1 \times 1$ nm$^3$. The adopted magnetic parameters[36,37] are the saturation magnetization $M_S = 5.8 \times 10^5$ A/m, exchange stiffness coefficient $A = 1.5 \times 10^{-11}$ J/m, Gilbert damping constant $\alpha = 0.01$ and uniaxial magnetocrystalline anisotropy $K_u = 0.8 \times 10^6$ J/m$^3$. The schematic diagram of the magnetic system structure is depicted in Fig. 1(a), with the inset illustrating the coordinate axes. The white arrows represent the magnetization direction of DW and the uniform magnetized blocks. The white circles with a white dot/cross on both ends of the nanowire present the magnetization direction. The purple arrow represents the direction of spin-wave propagation. A Bloch-type magnetic DW is set in the middle of the nanowire. To ensure that the position of the DW remains stationary under the driving of SWs, two triangular notches are symmetrically set at the edges of the nanowire in the region where the DW is located to implement pinning the DW. Here, we employ a Bloch-type DW because in subsequent sections of this study, it is intended to manipulate the forced oscillations of the DW through a localized Oersted field distributed along the $x$-direction. The magnetization within a Bloch-type DW is oriented along the $y$-direction, which facilitates more pronounced vibrational responses under the influence of an $x$-directional magnetic field. In the structure shown in Fig. 1(a), the nanowire length is significantly greater than its width and thickness, resulting in substantial shape anisotropy along the $x$-axis. This anisotropy facilitates the formation of a Néel-type DW.[17,30] To establish a stable Bloch-type DW, two uniformly magnetized nanostrips are set symmetrically on either side of the nanowire's midpoint along the $y$-axis for DW pinning (as illustrated in Fig. 1(a)). This configuration leverages the stray field along the $y$-axis to pin the magnetization within the DW, thereby ensuring its stability. Moreover, the presence of this stray field can further enhance the uniformity of the magnetization inside the DW. The SW antenna is positioned on the left side of the nanowire. The SW is excited by applying an alternating magnetic field along the $y$-direction within the antenna region. To facilitate the observation of the results, three observation zones (CZ1, CZ2 and CZ3), each with dimensions of $10 \times 20 \times 1$ nm$^3$, are set along the nanowire, as presented in Fig. 1(a). All spectral analyses in this study are conducted by performing a fast Fourier transform (FFT) on the time-dependent magnetization within the observation zones.

## 3. Results and discussion

Figure 1(b) presents a snapshot of the $x$-component of the magnetization distribution at a specific moment during the SW propagation along the nanowire at a frequency of 28 GHz. In this figure, red represents the $m_x$ (magnetization component along the $x$-axis) pointing in the positive $x$-direction, and blue the negative $x$-direction. The wavelength of the SW is approximately 40 nm. If the width of the DW is ignored, it can be observed that upon passing through the DW, the phase of the SW undergoes a 180° shift, which is consistent with the findings reported in the literature.[15]

To achieve high-quality MFCs, it is essential to investigate the propagation characteristics of SWs that aid in determining the suitable frequency ($f_0$) and amplitude ($h_0$) of the SW source. We studied the dispersion relationship of spin waves to determine their cutoff frequency. The specific method is to apply a sinc-function magnetic field $h_d(t) = A[\sin(2\pi f_d t)/(2\pi f_d t)]\hat{y}$ over the regions of the antenna on the left side of the nanowires to excite SWs with a wide frequency range, where $A = 60$ mT and $f_d = 50$ GHz. This approach

enables a continuous-band excitation, allowing us to extract the dispersion relation without multiple narrow-band sweeps. Similar broadband excitation schemes are widely used in SW and optical spectroscopy for efficient mapping of frequency-dependent responses.[1,38,39] The color dispersion curve is obtained by performing a 2D fast Fourier transform (FFT) of the temporal $m_y(x,t)$ in space and time, as shown in Fig. 1(c). The horizontal axis represents the wave vector $\boldsymbol{k}$, and the vertical axis represents the frequency of the SW ($f_{\rm SW}$). The results show that the cutoff frequency $f_{\rm min}$ is about 25 GHz.

In addition to the cutoff frequency, the excitation efficiency of SWs is also crucial. We need to obtain larger $h_0$ with smaller magnetic field disturbances, that is, to find the resonant frequency of SWs. We initially explored the propagation characteristics of the SWs in a nanowire with uniform magnetization along the $z$-axis, that is, in the absence of a DW. A driving magnetic field $h(t) = h_0\cos(2\pi f_0 t)\hat{y}$ is introduced, with $h_0 = 60$ mT and the value of $f_0$ ranges from 26 GHz to 35 GHz. Figure 1(d) illustrates the amplitude of the excited SWs ($h_{\rm SW}$) under the driving magnetic field at various frequencies, which is derived from the variation of the $y$-component of the magnetic moment ($m_y$) in CZ1. As $f_0$ increases, $h_{\rm SW}$ exhibits periodic fluctuations. When $f_{\rm SW}$ reaches 28 GHz, the SWs demonstrate large amplitude and enhanced temporal stability. Based on the findings in Figs. 1(c) and 1(d), and with the aim of generating more frequency comb teeth, we will focus on the frequency range of $f_{\rm SW}$ between 28 GHz to 32 GHz in the subsequent research of this study.

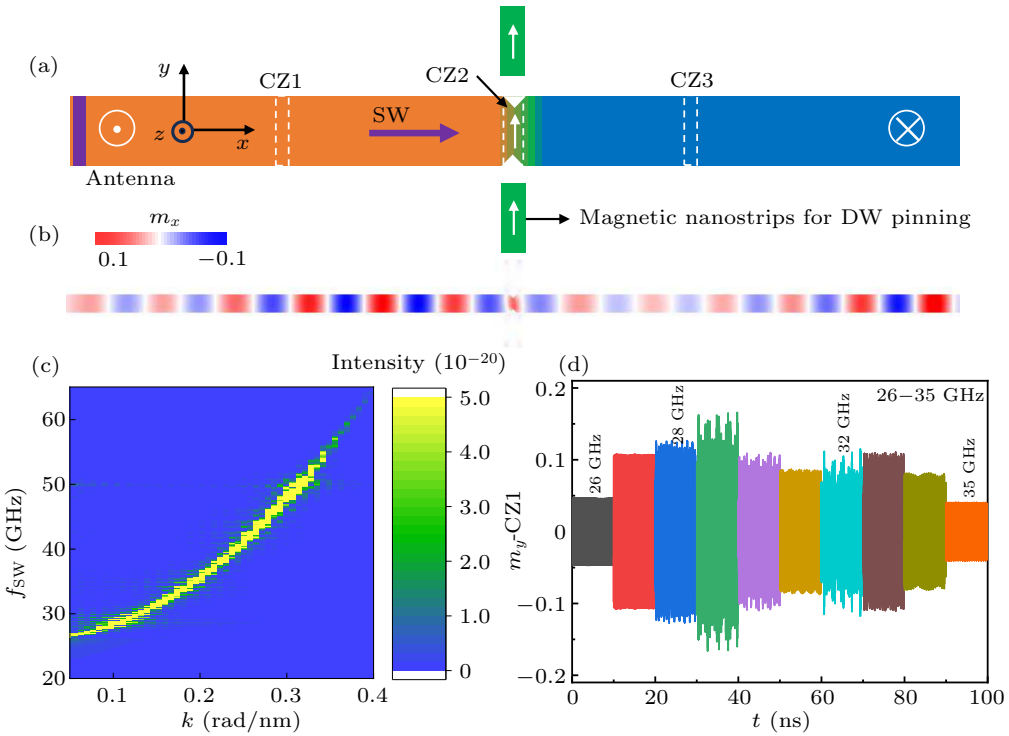



**Fig. 1.** Propagation characteristics of the SW. (a) Schematic diagram of the magnetic system structure. (b) Snapshot of the $x$-component of the magnetization distribution during the SW propagation along the nanowire at a frequency of 28 GHz. (c) Dispersion relation obtained by performing a 2D FFT of the temporal $m_y(x,t)$ distribution under sinc-function magnetic field excitation. Color map represents the spin-wave intensity, revealing the intrinsic spin-wave modes supported by the nanowire structure. (d) Variation of $h_{\rm SW}$ under the driving magnetic field at different frequencies, observed from the $m_y$ in CZ1.

The SWs propagate in the positive $x$-axis direction and subsequently interact with the DW, inducing oscillation. Figure 2(a) illustrates the frequency spectrum of the magnetic moment vibration within the DW, which was obtained via FFT. The FFT is applied to the three normalized magnetization components ($m_x$, $m_y$ and $m_z$) of the time-varying magnetization in CZ2. Interestingly, it is observed that the vibration frequencies of $m_x$ and $m_z$ are both 2.065 GHz, while the frequency of $m_y$ is 4.132 GHz, which is exactly twice that of the former two. This observation is further corroborated by the time-domain waveforms of the three magnetization components depicted in Fig. 2(b). This double-frequency phenomenon can be attributed to the Bloch DW being subjected to a $y$-directional stray field. Under the SW perturbation, the magnetization direction inside the DW deviates from the $y$-axis direction. However, since the stray field remains fixed along the $y$-axis, a magnetization precession occurs around this axis. During each precession cycle, $m_x$ and $m_z$ oscillate between positive and negative values, while $m_y$, being significantly larger than $m_x$ and $m_z$, does not pass through zero in its oscillation range. As a result, $m_y$ completes two cycles while $m_x$ and $m_z$ complete one, which explains why the vibration frequency of $m_y$ is twice that of $m_x$ and $m_z$.

The generation of the MFC relies on the coupling between the SW and oscillating DW. Exciting and controlling the vibration frequency of the DW ($f_{\rm DW}$) is the key to realizing

the frequency comb effect. The magnetic system discussed in this study employs a dual-pinning mechanism: notch pinning and stray field pinning. The former restricts the displacement of the DW, thereby circumventing the influence of the Doppler effect. Consequently, the observed DW vibration does not involve positional movement, but rather precession of the internal magnetization orientation around the localized stray field at the pinning site. This precession arises from the disturbance of the SW on the magnetization orientation inside the magnetic DW. Under this disturbance, the magnetization state within the DW deviates from the direction of the stray field, leading to precession. We utilize this precession to construct the vibration mode of the DW. Figure 2(c) shows the time-domain waveforms of $m_x$ and $m_y$ collected from CZ3 under a 28 GHz SW. The waveforms exhibit distinct modulation, indicating that the SWs contain multiple frequency components as they pass through the DW. Figure 2(d) displays the spectral curves obtained by performing an FFT on the $m_x$ in CZ3 with the $h_{\mathrm{SW}}$ varying from 40 mT to 120 mT and the $f_{\mathrm{SW}}$ set at 28 GHz. A distinct spectrum feature of the frequency comb can be seen. At $h_0 = 40$ mT, only the frequency consistent with $f_{\mathrm{SW}}$ is observed. This is attributed to the weak energy of the SW, which is insufficient to drive the vibration of the DW, thereby precluding the formation of a frequency comb. When $h_0$ ranges from 60 mT to 80 mT, the DW vibration is excited, generating a frequency comb. The comb spacing matches the $f_{\mathrm{DW}}$ in the spectral curve of CZ3, with the comb teeth corresponding to the sum and difference frequencies of $f_{\mathrm{SW}}$ and $f_{\mathrm{DW}}$. The interval between the comb teeth is $f_{\mathrm{DW}}$. At higher amplitudes ($h_0 = 100$ mT and 120 mT), as shown in Fig. 2(d), spurious peaks emerge in the frequency comb due to the nonlinear oscillation of the DW under intense SWs, a phenomenon consistent with findings in the literature.[14,24]

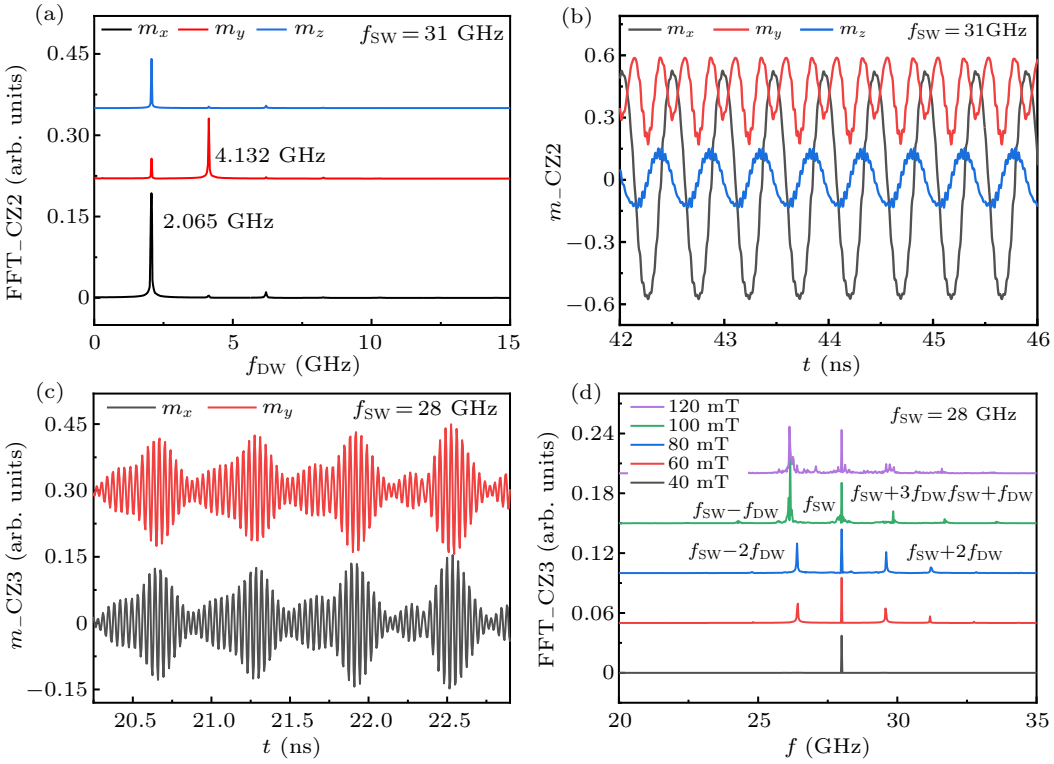



**Fig. 2.** Frequency comb formed by SW-driven DW vibration. (a) Frequency spectrum of the DW vibration driven by SW. (b) Time-domain waveforms of the three magnetization components of the DW. (c) Time-domain waveforms of $m_x$ and $m_y$ collected from CZ3, driven by a 28 GHz SW. (d) Frequency spectrum curves obtained by performing an FFT on $m_x$ in CZ3 as $h_0$ varies from 40 mT to 120 mT.

Regarding the physical mechanism of the frequency comb generation, existing publications generally attribute it to the three-magnon or four-magnon process between the SW and the magnetic textures.[6,7,9,12,14,31,34] From the perspective of wave dynamics, we can also explain that the magnetic moment oscillation induced by SWs couples with the intrinsic oscillation of the DW, which can be understood as a multiplication process. The coupled magnetic moment vibration can be described by the equation

$$m(t) = h_{\mathrm{SW}} \cos(2\pi f_{\mathrm{SW}} t) \cdot h_{\mathrm{DW}} \cos(2\pi f_{\mathrm{DW}} t). \quad (1)$$

Here, $h_{\mathrm{SW}}$ and $h_{\mathrm{DW}}$ represent the amplitudes of the SW and DW oscillations, respectively, while $f_{\mathrm{SW}}$ and $f_{\mathrm{DW}}$ denote their respective frequencies. After performing the straightforward calculations, Eq. (1) can be rewritten as

$$m(t) = \frac{1}{2} h_{\mathrm{SW}} \cdot h_{\mathrm{DW}} \left[\cos(2\pi(f_{\mathrm{SW}} + f_{\mathrm{DW}})t) + \cos(2\pi(f_{\mathrm{SW}} - f_{\mathrm{DW}})t)\right]. \quad (2)$$

In Eq. (2), equal-amplitude sum and difference frequency components appear. These composite frequency components, including fundamental and harmonic frequencies undergo fur-

ther multi-path reflection and repeated coupling with DW. This process ultimately results in a series of frequency comb spectra characterized by $f_{SW}$ as the fundamental frequency and $f_{DW}$ as the spacing between the comb teeth. The oscillating DW, coupled with SWs, can be regarded as a new SW source.[4,13,29] From this source, the SWs propagated bidirectionally along the nanowire, manifesting as both transmitted and reflected waves. It can be inferred that the SWs propagating to the left will superimpose with the original SW, forming a new mode for the frequency comb.

The tunability of the comb spacing is crucial for the frequency comb application. We have noticed that $f_{DW}$ is much lower than the SW, indicating that the DW vibrates at its intrinsic frequency. This intrinsic frequency is influenced by both the structural and material parameters of the nanowire and the characteristics of the SW including $f_{SW}$ and $h_{SW}$. In the proposed frequency comb based on DWs, the vibration of the DW is fundamentally attributed to the Larmor precession of the internal magnetization orientation around the local stray field. According to magnetic theory, the Larmor precession frequency[40] is given by

$$f = \gamma \boldsymbol{H}. \tag{3}$$

Here, $\gamma$ is the gyromagnetic ratio of the magnetic system and $\boldsymbol{H}$ is the external magnetic field, which is the superposition of the local stray field and the effective fields introduced by the SW. When the model parameters are fixed, $f_{DW}$ may be influenced by $f_{SW}$ and $h_{SW}$, as well as the local stray field.

Figure 3(a) displays the frequency spectrum of the DW oscillation, obtained by performing an FFT on $m_x$ in CZ2 under the influence of SWs with various amplitudes and a fixed $f_{SW}$ of 28 GHz. It is observed that within the range of $h_0 = 40$ mT to 120 mT, there is no significant trend in $f_{DW}$. However, when $h_0$ reaches 120 mT, the DW exhibits high-order nonlinear oscillations, leading to a broadened oscillation spectrum. Figure 3(b) illustrates the frequency spectrum of the DW oscillation in CZ2 under the influence of SWs with a fixed $h_0$ of 60 mT and various frequencies. Similar to the results shown in Fig. 3(a), there is no significant trend in $f_{DW}$.

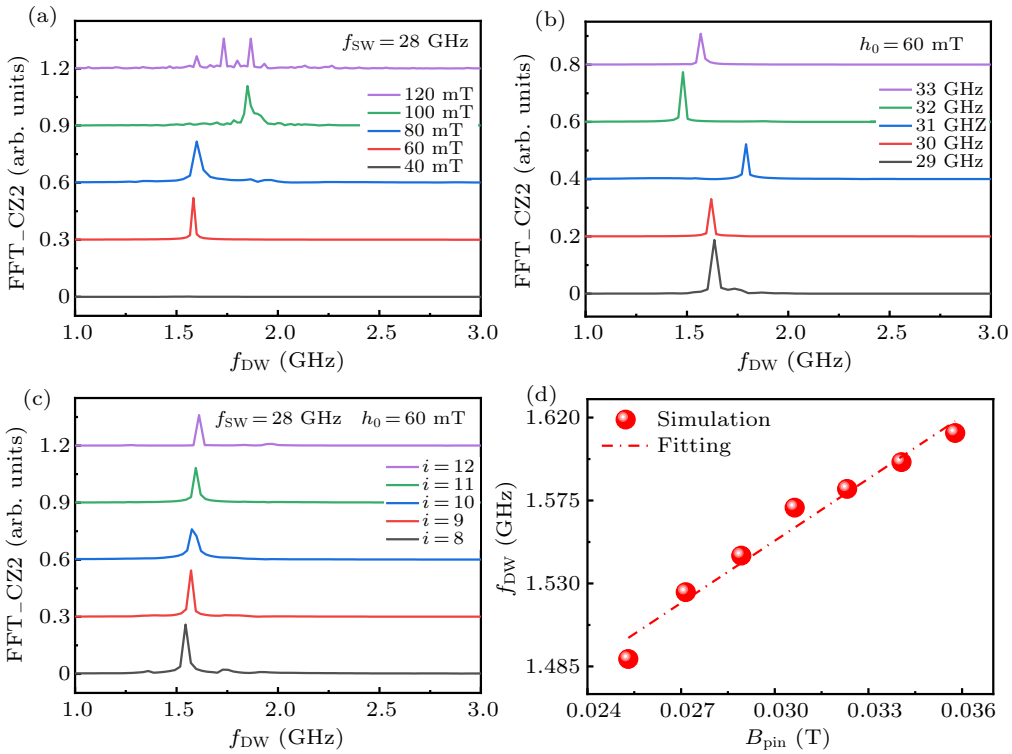



**Fig. 3.** Influence of the stray fields on the intrinsic oscillation frequency of the DW. (a) $f_{DW}$ under the action of various $h_0$. (b) $f_{DW}$ under the influence of various $f_{SW}$. (c) $f_{DW}$ under different $M_S$ of the magnetic nanostrips. (d) Larmor precession frequency of the DW varies with the strength of the stray fields.

Given these observations, it is reasonable to infer that $f_{DW}$ is closely related to the stray field. In our simulation model, the DW is pinned by the stray field ($B_{pin}$) generated from two uniformly magnetized nanostrips along the $y$-axis. By adjusting $B_{pin}$, we investigate the precession frequency of the DW. The strength of $B_{pin}$ can be controlled experimentally by altering the thickness of the magnetic nanostrips. In simulations, however, the $B_{pin}$ can be adjusted by modifying the saturation magnetization $M_S$ of the magnetic nanostrips. In this simulation, $M_S$ is set as $M_S = 8.5 \times 10^5 \times (0.5 + i \times 0.05)$, where $i$ is the adjustment coefficient. Figure 3(c) presents the spectral curves of the DW as $i$ varies from 8 to 12. It is evident that the intrinsic frequency $f_{DW}$ increases with the increase in $M_S$. To quantitatively characterize the relationship between the stray field and $f_{DW}$, we extract the stray field at the center of the magnetic nanostrips at the $+y$ side and calculate $f_{DW}$ using

FFT. As shown in Fig. 3(d), modulating the stray field can significantly influence $f_{DW}$. Within a specific range of $B_{pin}$, the relationship between $f_{DW}$ and the stray field strength is approximately linear, as evidenced by the fitting results. This observation is consistent with the theoretical description provided in Eq. (3).

The research described above reveals that, under the disturbance of the SWs, the magnetic moments within the DW process around the stray field are affected by the Larmor frequency. The interaction between the SW and the precessing DW generates a frequency comb, with the comb's spacing determined by the DW's precession frequency. To control the comb spacing, modulating the Larmor precession frequency is necessary, which typically involves altering the structural and material parameters of the magnetic system. However, these indirect methods are influenced by multiple factors and lack precision, rendering them unsuitable for real-time device operation and posing significant challenges for the practical implementation of the frequency comb.

Here, we propose a method for driving DW vibrations using the Oersted field generated by an alternating current in a localized nanoscale region. By adjusting the frequency ($f_{AC}$) and amplitude ($h_{AC}$) of the driving current, the $f_{DW}$ can be directly controlled. This approach enables precise regulation of the DW spacing, avoiding the uncertainties associated with applying a global oscillating external magnetic field.

As shown in Fig. 4(a), a current-carrying wire perpendicular to the $XZ$ plane was placed 2 nm below the nanowire. The alternating Oersted field generated by the alternating current flowing through the wire drives the DW vibration. Figure 4(b) displays the distribution of the Oersted field in the nanowire produced by a direct current of 0.1 mA, where the solid and dashed blue curves represent the $x$- and $z$-components of the Oersted field ($B_x$ and $B_z$), respectively. Notably, the Oersted field, has no $y$-component and exhibits prominent localized distribution characteristics, with the strongest magnetic field near the DW gradually decaying with increasing distance. The inset of Fig. 4(b) shows the $f_{DW}$ driven by a 2 GHz alternating current (0.1 mA). The DW undergoes forced vibration driven by the Oersted field, with its vibration frequency matching $f_{AC}$. Figure 4(c) presents the frequency spectrum curves of $m_x$ in regions CZ1 and CZ3 under a 32 GHz SW and 2 GHz alternating current (0.1 mA).

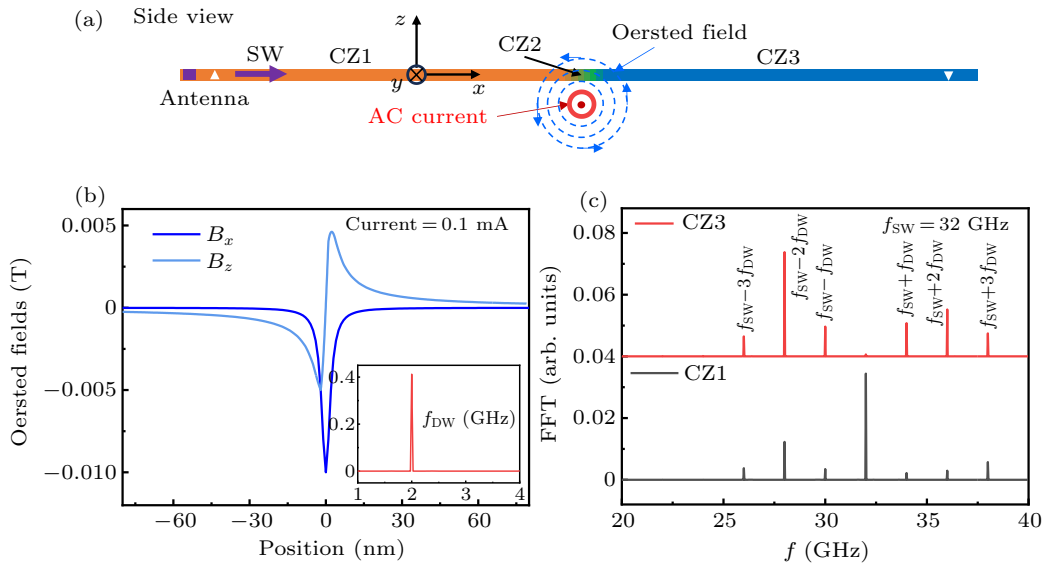



**Fig. 4.** Frequency comb generated by Oersted field-driven DW vibration. (a) Schematic diagram (side view) of the magnetic system structure. Red circle with a dot represents the current-carrying wire perpendicular to the $XZ$ plane. Dashed blue line with arrows indicates the Oersted field and its direction. (b) Distribution of the Oersted field in the nanowire produced by a direct current of 0.1 mA. Inset shows the $f_{DW}$ under a 2 GHz alternating current (0.1 mA). (c) Frequency comb effects in regions CZ1 and CZ3, featuring a central peak at 32 GHz with 2 GHz spacing.

The results in Fig. 4(c) confirm that the vibrating DW acts as a wave source, transmitting composite frequency components generated by the coupling effect to both sides of the nanowire. Frequency comb effects are observed in both regions CZ1 and CZ3, with a central peak at 32 GHz and a spacing of 2 GHz. Interestingly, unlike the frequency comb in CZ1, the amplitude of the central frequency in the frequency comb in CZ3 is canceled out. This phenomenon can be attributed to the constructive or destructive interference generated by the reflection of SWs at the nanowire's boundary and their superposition with the original traveling waves. By changing the position of the observation areas, we can obtain frequency comb spectra with different constructive or destructive features. This can be confirmed from Fig. 1(b), where the brightness of the blue or red regions representing $h_{SW}$ varies in different areas of the nanowire, indicating that the intensity of SWs is unevenly distributed along the nanowire.

When $f_{AC}$ deviates significantly from the intrinsic $f_{DW}$, a stronger magnetic field is required to sustain its forced vibration of the DW. In addition, due to the presence of the in-

trinsic frequency, high-order frequency components from the nonlinear responses may emerge in $f_{DW}$,[4,21,24,25,29] thus introducing noise into the frequency comb. To verify this conclusion, we varied $f_{AC}$ with a step of 0.1 GHz and investigated the vibration behavior of the DW and its frequency comb effect under different $f_{AC}$ values. Figure 5(a) illustrates the $m_x$ frequency spectrum curves in CZ2 at a $f_{SW}$ of 32 GHz for various $f_{AC}$. It is evident that as $f_{AC}$ changes, the $f_{DW}$ exhibits pronounced forced vibration characteristics and remains consistent with $f_{AC}$. When $f_{AC}$ is within the range of 2 GHz to 2.4 GHz, the $f_{DW}$ exhibits only one characteristic peak in its frequency spectrum since its intrinsic vibration frequency is 2.065 GHz, closely matching $f_{AC}$. However, when $f_{AC}$ deviates significantly, such as at 1.9 GHz, the DW exhibits nonlinear oscillations, resulting in additional frequency peaks in the spectrum beyond $f_{AC}$.

Figure 5(b) presents the frequency combs observed in CZ3 under various $f_{AC}$ values. All frequency combs exhibit a clean background, except where $f_{AC}$ is 1.9 GHz. The black dashed line indicates the location of the disappearing fundamental frequency of the SW. The comb spacing of the frequency comb is determined by $f_{DW}$. When the DW oscillation includes harmonic or subharmonic components of the driving current, the frequency comb exhibits corresponding comb spacing.

The results in Fig. 5(a) indicate that under the action of the Oersted field generated by the alternating current, the DW exhibits typical forced vibration characteristics. However, when $f_{AC}$ is significantly different from the intrinsic $f_{DW}$, the DW undergoes nonlinear vibration, leading to the emergence of impurity peaks. It is reasonable to assume that the intensity of the Oersted field should also be carefully selected since a powerful Oersted field may also induce nonlinear oscillations in the magnetic DWs. Figures 5(c) and 5(d) illustrate the impact of $h_{AC}$ on $f_{DW}$ and the frequency comb effect, respectively. Variations in $h_{AC}$ do not affect the central frequency of $f_{DW}$. However, when $h_{AC}$ is too large, the fundamental frequency broadens, and high-order nonlinear oscillations occur. As the gray dashed line indicates, these high-order oscillation frequencies shift away from the fundamental frequency as the current intensity increases. As shown in Fig. 5(d), all the frequency components in $f_{DW}$ couple with $f_{SW}$ generated sum and different frequency components that become part of the frequency comb. Complex DW vibrations can confuse the frequency comb spectrum, which is not conducive to its application. The findings in Fig. 5 confirm that by selecting appropriate $f_{AC}$ and $h_{AC}$, a high-quality and comb-spacing tunable MFC based on DW can be achieved.

It is worth noting that in this study, we found that high-amplitude or off-resonant conditions may offer interesting possibilities for tuning comb characteristics. Although the current manuscript focuses on the spectral behavior under resonant conditions, the emergence of sub-comb structures and sideband components in detuned regimes indeed suggests potential for high-resolution frequency control.

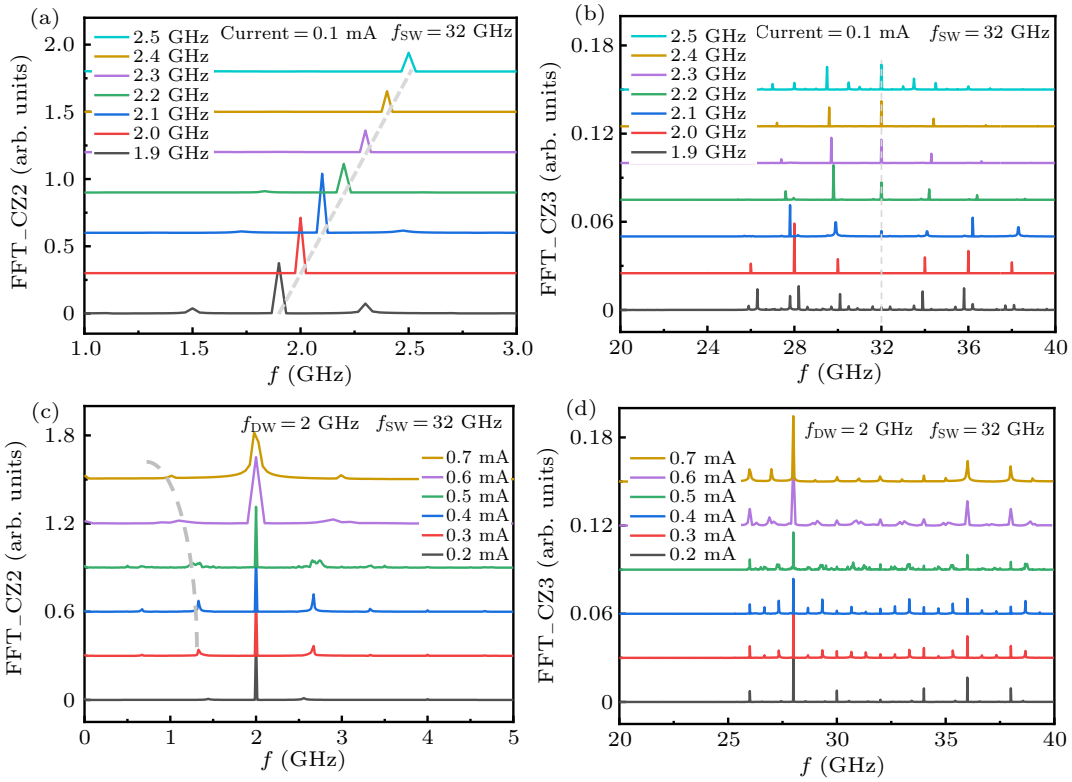



**Fig. 5.** Influence of current frequency and amplitude on the frequency comb. (a) $m_x$ frequency spectrum in CZ2 with a $f_{SW}$ of 32 GHz for various current frequencies. (b) Frequency combs observed in CZ3. (c) Impact of $h_{AC}$ on $f_{DW}$. (d) Impact of $h_{AC}$ on the frequency comb effect.

## 4. Conclusion

We proposed an MFC based on DW with directly tunable comb spacing. A Bloch-type DW with stable structure and position was formed using a dual-pinning method that combines artificial structural defects with stray fields. The DW vibration mode with Larmor precession was constructed to achieve the frequency comb effect. Our research results indicate that under the action of local stray fields and the effective perturbation magnetic field caused by traveling SWs, the magnetic moment inside the DW continuously precesses around the stray field, thus generating DW oscillations with the Larmor frequency as the intrinsic frequency. The oscillating DW couples with SWs to form a frequency comb, where the comb spacing can be precisely controlled by adjusting the strength of the locally distributed stray field. We further utilized the locally distributed Oersted field generated by alternating current to induce forced vibration of the DW, enabling direct control over the frequency comb spacing. Our research findings indicate that, in the forced vibration mode of DW, the frequency comb spacing can be precisely controlled by adjusting the frequency of the alternating current within the range near the natural vibration frequency of the DW. In contrast, the amplitude variation of AC current has no significant influence regulation of the frequency comb. This study provides a useful and effective method for regulating the magnon frequency comb, which will be of potential value and should play a significant role in the design of spintronic devices, spin-wave calibration, spin-wave excitation, precise detection of topological defects, and even in magnetic oscillator lasers and quantum computing.[6]

## Acknowledgements

This study was supported by the National Natural Science Foundation of China (Grant No. 12364020), the Scientific and Technological Development Plan of Jilin Province (Grant No. 20240101295JC), the Science and Technology Research and Planning Project of Jilin Provincial Department of Education (Grant No. JJKH20230611KJ), and the Applied Foundation Research Project (Talent Funding Project) of Yanbian University (Grant No. ydkj202241).

## References

[1] Wang Z, Cao Y, Yan P, Wang X R and Zhang B 2018 *Phys. Rev. B* **97** 094421
[2] Xiong H 2023 *Fundam. Res.* **3** 8
[3] Matveeva P G and Aristov D N 2016 *Phys. Rev. B* **94** 214425
[4] Van de Wiele B, Hämäläinen S J, Baláž P, Montoncello F and van Dijken S 2016 *Sci. Rep.* **6** 21330
[5] Fernández-García L, Ruiz-Gómez S, Guerrero R, Guedas R, Aroca C, Perez L, Prieto J L and Muñoz M 2024 *APL Mater.* **12** 051116
[6] Zheng S, Wang Z, Wang Y, Sun F, He Q, Yan P and Yuan H Y 2023 *J. Appl. Phys.* **134** 151101
[7] Schultheiss K, Hula T, Verba R, Fassbender J, Kákay A, Schultheiss H and Körber L 2020 *Phys. Rev. Lett.* **125** 207203
[8] Yu H, Xiao J and Schultheiss H 2021 *Phys. Rep.* **905** 1
[9] Liang X, Cao Y, Yan P and Zhou Y 2024 *Nano Lett.* **24** 6730
[10] Sun J, Shi S and Wang J 2022 *Adv. Eng. Mater.* **24** 2101245
[11] Wang Z, Yuan H Y, Cao Y, Li Z X, Duine R A and Yan P 2021 *Phys. Rev. Lett.* **127** 037202
[12] Wang Z, Yuan H Y, Cao Y and Yan P 2022 *Phys. Rev. Lett.* **129** 107203
[13] Ge X, Chen Y, Cao Y, Li C, Li T, Li Z, You L, Liang S, Yang X and Zhang Y 2022 *J Phys. D: Appl. Phys.* **55** 295302
[14] Zhou Z, Wang X, Nie Y, Xia Q and Guo G 2021 *J. Magn. Magn. Mater.* **534** 168046
[15] Hertel R, Wulfhekel W and Kirschner J 2004 *Phys. Rev. Lett.* **93** 257201
[16] Zhang S, Mu C, Zhu Q, Zheng Q, Liu X, Wang J and Liu Q 2014 *J. Appl. Phys.* **115** 013908
[17] Chang L, Liu Y, Kao M, Tsai L, Liang J and Lee S 2018 *Sci. Rep.* **8** 3910
[18] Gao Z, Su Y, Weng L, Hu J and Park C 2019 *New J. Phys.* **21** 063014
[19] Djuhana D, Piao H, Lee S, Kim D, Ahn S and Choe S 2010 *Appl. Phys. Lett.* **97** 022511
[20] Djuhana D, Soegijono B, Piao H, Oh S K, Yu S and Kim D 2013 *J. Korean Phys. Soc.* **63** 654
[21] Dong X and Wu Z 2024 *Chin. Phys. B* **33** 067502
[22] Cheng M, Yuan X, Li S, Chen C, Zhang Z, Yu Z, Liu Y, Lu Z and Xiong R 2020 *Nanotechnology* **31** 235201
[23] Berger L 1986 *Phys. Rev. B* **33** 1572
[24] Bisig A, Heyne L, Boulle O and Kläui M 2009 *Appl. Phys. Lett.* **95** 162504
[25] Han D, Kim S, Lee J, Hermsdoerfer S J, Schultheiss H, Leven B and Hillebrands B 2009 *Appl. Phys. Lett.* **94** 112502
[26] Metaxas P J, Albert M, Lequeux S, Cros V, Grollier J, Bortolotti P, Anane A and Fangohr H 2016 *Phys. Rev. B* **93** 054414
[27] Martinez E, Torres L and Lopez-Diaz L 2011 *Phys. Rev. B* **83** 174444
[28] Singh B, Ravishankar R, Otálora J A, Soldatov I, Schäfer R, Karnaushenko D, Neu V and Schmidt O G 2022 *Nanoscale* **14** 13667
[29] Arai H, Tsukahara H and Imamura H 2012 *Appl. Phys. Lett.* **101** 092405
[30] Franken J H, Lavrijsen R, Kohlhepp J T, Swagten H J M and Koopmans B 2011 *Appl. Phys. Lett.* **98** 102512
[31] Hula T, Schultheiss K, Gonçalves F J T, Körber L, Bejarano M, Copus M, Flacke L, Liensberger L, Buzdakov A, Kákay A, Weiler M, Camley R, Fassbender J and Schultheiss H 2022 *Appl. Phys. Lett.* **121** 112404
[32] Luo X, Lu Z, Yuan C, Guo F, Xiong R and Shi J 2016 *J. Appl. Phys.* **119** 233901
[33] Rao J W, Yao B, Wang C Y, Zhang C, Yu T and Lu W 2023 *Phys. Rev. Lett.* **130** 046705
[34] Verba R, Wehrmann F, Wagner K, Körber L, Hula T, Hache T, Kákay A, Awad A A, Tiberkevich V, Slavin A N, Fassbender J, Schultheiss H and Schultheiss K 2019 *Phys. Rev. Lett.* **122** 097202
[35] Vansteenkiste A, Leliaert J, Dvornik M, Helsen M, Garcia-Sanchez F and Van Waeyenberge B 2014 *AIP Adv.* **4** 107133
[36] Sampaio J, Cros V, Rohart S, Thiaville A and Fert A 2013 *Nat. Nanotechnol.* **8** 839
[37] Yang X, Ai X, Liu X, Li H, Ma X, Shim J and Piao H 2024 *Appl. Phys. Lett.* **125** 172403
[38] Venkat G, Kumar D, Franchin M, Dmytriev O, Mruczkiewicz M, Fangoh H, Barman A, Krawczyk M and Prabhakar A 2013 *IEEE Trans. Magn.* **49** 524
[39] Wang Q, Chumak A, Jin L, Zhang H, Hillebrands B and Zhong Z 2017 *Phys. Rev. B* **95** 134433
[40] Holmqvist C, Belzig W and Fogelstrom M 2018 *Philos. Trans. R. Soc. A* **376** 20150229